AFRL-AFOSR-UK-TR-2013-0013

Three dimensional optical metamaterials via direct laser writing

Maria Farsari

Foundation for Research and Technology Hellas (FORTH)
N. Plastira 100, Vassilika Vouton
Heraklion, Greece 70013

EOARD Grant 11-3090

Report Date: March 2013

Final Report for 01 October 2011 to 30 September 2012

Air Force Research Laboratory
Air Force Office of Scientific Research
European Office of Aerospace Research and Development
Unit 4515 Box 14, APO AE 09421

REPORT DOCUMENTATION PAGE

Form Approved OMB No. 0704-0188

1. REPORT DATE *(DD-MM-YYYY)*	2. REPORT TYPE	3. DATES COVERED *(From – To)*
21 March 2013	Final Report	1 October 2011 – 30 September 2012

4. TITLE AND SUBTITLE

Three dimensional optical metamaterials via direct laser writing

5a. CONTRACT NUMBER

FA8655-11-1-3090

5b. GRANT NUMBER

Grant 11-3090

5c. PROGRAM ELEMENT NUMBER

61102F

6. AUTHOR(S)

Maria Farsari

5d. PROJECT NUMBER

5d. TASK NUMBER

5e. WORK UNIT NUMBER

7. PERFORMING ORGANIZATION NAME(S) AND ADDRESS(ES)

Foundation for Research and Technology Hellas (FORTH)
N. Plastira 100, Vassilika Vouton
Heraklion, Greece 70013

8. PERFORMING ORGANIZATION REPORT NUMBER

N/A

9. SPONSORING/MONITORING AGENCY NAME(S) AND ADDRESS(ES)

EOARD
Unit 4515 BOX 14
APO AE 09421

10. SPONSOR/MONITOR'S ACRONYM(S)

AFRL/AFOSR/IOE (EOARD)

11. SPONSOR/MONITOR'S REPORT NUMBER(S)

AFRL-AFOSR-UK-TR-2013-0013

12. DISTRIBUTION/AVAILABILITY STATEMENT

Distribution A: Approved for public release; distribution is unlimited.

13. SUPPLEMENTARY NOTES

14. ABSTRACT

In this report we describe our research into the fabrication of fully three-dimensional metallic metamaterials using Diffusion-Assisted Direct Laser Writing, a novel technique which employs quencher diffusion to fabricate structures with resolution beyond the diffraction limit. We have made dielectric 3D nanostructures by multiphoton polymerization using a metal-binding organic-inorganic hybrid material, and we covered them with silver using selective electroless plating. We have used this method to make spirals and woodpiles with 600 nm intralayer periodicity. The resulting photonic nanostructures have a smooth metallic surface and exhibit well-defined diffraction spectra, indicating good fabrication quality and internal periodicity. In addition, we have made dielectric woodpile structures decorated with gold nanoparticles. Our results show that Diffusion-Assisted Direct Laser Writing and selective electroless plating can be combined to form a viable route for the fabrication of 3D dielectric and metallic photonic nanostructures.

15. SUBJECT TERMS

EOARD, Nonlienan Optical Wave Equation, Nano-structed Media, Nonlinear Fiber Lasers

16. SECURITY CLASSIFICATION OF:			17. LIMITATION OF ABSTRACT	18, NUMBER OF PAGES	19a. NAME OF RESPONSIBLE PERSON
a. REPORT	b. ABSTRACT	c. THIS PAGE			John Gonglewski
UNCLAS	UNCLAS	UNCLAS	SAR	18	19b. TELEPHONE NUMBER *(Include area code)* +44 (0)1895 616007

Title: Three dimensional optical metamaterials via direct laser writing

Maria Farsari, IESL-FORTH, N. Plastira 100, Heraklion, Crete, Greece

In this report we describe our research into the fabrication of fully three-dimensional metallic metamaterials using Diffusion-Assisted Direct Laser Writing, a novel technique which employs quencher diffusion to fabricate structures with resolution beyond the diffraction limit. We have made dielectric 3D nanostructures by multiphoton polymerization using a metal-binding organic-inorganic hybrid material, and we covered them with silver using selective electroless plating. We have used this method to make spirals and woodpiles with 600 nm intralayer periodicity. The resulting photonic nanostructures have a smooth metallic surface and exhibit well-defined diffraction spectra, indicating good fabrication quality and internal periodicity. In addition, we have made dielectric woodpile structures decorated with gold nanoparticles. Our results show that Diffusion-Assisted Direct Laser Writing and selective electroless plating can be combined to form a viable route for the fabrication of 3D dielectric and metallic photonic nanostructures.

The Direct Laser Writing technique and its advances in the framework of the project

Direct Laser Writing (DLW) by multiphoton polymerization (MPP) has become a powerful tool for the fabrication of fully three-dimensional micro- and nano-structures for microfluidic, biomedical, metamaterial, and photonic applications.[1] In DLW, the beam of an ultrafast laser is tightly focused into the volume of a photosensitive material, initiating multiphoton polymerization within the focused beam voxel. By moving the focus of the beam three-dimensionally, arbitrary 3D, high-resolution structures can be written into the volume of the material. By simply immersing the sample in an appropriate solvent, the unscanned, unpolymerized area can be dissolved, revealing the 3D structure.

While DLW is fundamentally the only technique available that can produce readily assembled, fully 3D micro and nanostructures, its resolution lags behind other competing technologies such as e-beam lithography, where tens of nanometers are routinely achieved. Recently, there has been a lot of research effort to improve this resolution. One method is the use of an inhibiting molecule, such as a quencher, in the photopolymerizable material. In general, photopolymerization is a light-induced reaction which converts a monomer into a solid polymer. This reaction requires the use of an appropriate photoinitiator, a light sensitive molecule that produces a radical upon irradiation. It is a popular misconception that the highest resolution that can be achieved by a focused light beam is given by Abbe's diffraction limit. In fact, this is only valid in reversible, non-invasive procedures, such as imaging. When there is permanent modification of the sample, like in photopolymerization, then there is more than one process involved. To start with, when absorbing the light, the photoinitiator becomes excited and produces radicals; these radicals attack monomer molecules to form macroradicals of the polymer. Finally, the radicals are terminated to give the polymer. Radical termination can be also induced by oxygen and other molecules in the system, known

as scavengers. Quenching competes with photopolymerization and is usually considered detrimental to the process. In multiphoton photopolymerization, however, it can be used to circumvent the diffraction limit and produce structures of very high resolution. This can be done by modifying the light intensity at the focal point so that the light-produced radicals, whose spatial concentration is proportional to the square of the light intensity, exceed the quenchers and initiate polymerization only at the area where the exposure energy is larger than the threshold. In this case, the diffraction limit becomes just a measure of the focal spot size and it does not really determine the polymerization voxel size (Fig. 1a).

While, however, oxygen or additional quenchers reduce the absolute number of radicals, it should be possible to achieve a similar effect by simply reducing the laser power. Indeed, efforts to date to improve resolution using quenchers have marginally increased the resolution of single, suspended lines. However, they have not produced any high resolution 3D structures. More importantly, they have not reduced the distance between high resolution lines. As described in detail by Fischer and Wegener[2], the biggest challenge in DLW not yet addressed is not in the creation of sub-diffraction features, but sub-diffraction gaps between features. When attempting to form two features at sub-diffraction distance, the polymerization threshold is also exceeded in the interstice between the features due to the diffraction-limited widths of the absorbed energy distributions (Fig. 1b). This is a geometrical effect that cannot be easily overcome by any physical or chemical mechanism providing the polymerization threshold. A non-diffusing quencher simply increases the polymerization threshold, as the absorbed photons are partly wasted to neutralize the quencher. Diffusion of the free radical can make the spatial resolution even worse by causing indirect polymerization even in unexposed areas.

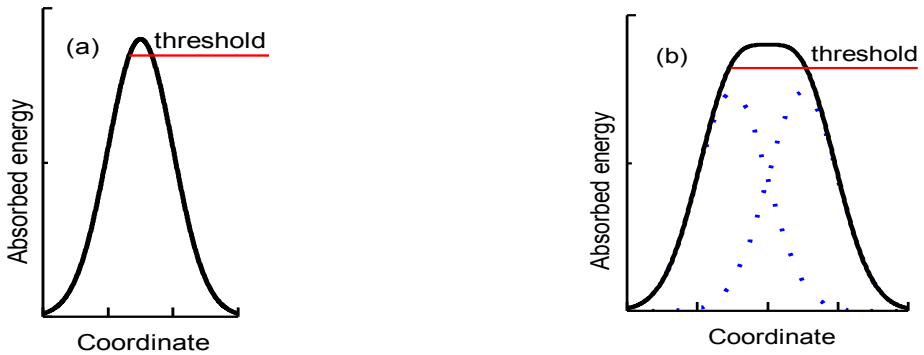

Figure 1 (a) Formation of a single sub-diffraction-sized feature is possible due to the polymerization threshold. (b) Formation of two features at sub-diffraction distance is limited by tails of the distributions of the energy absorbed during scans (blue dotted lines). The total absorbed energy (black line) exceeds the threshold not only where the nanofeatures are expected to form but also in the interstice.

One method which has successfully and substantially increased the resolution not only of single lines but also of structures is DLW inspired by stimulated-emission-depletion (STED) fluorescence microscopy[3]. In STED-DLW, two laser beams are used; one is used to generate the radicals, and the second beam to deactivate them. Several schemes have been proposed including single-photon (rather than multi-photon) excitation, a one-color scheme,

and multi-photon two-color scheme[2]. In addition to increasing the resolution, the possibility to shape the de-activating beam allows the very precise control of the voxel shape, and therefore the polymerization shape. Woodpiles with 350 nm intralayer periodicity and clear stopgaps have been fabricated using this method, while structures with 250 nm intralayer periodicity show evidence of stopgaps[2]. However, the implementation of DLW-STED is complicated, requiring very fine beam control and specialized photoinitiators which not only have high two-photon cross-section, but also high fluorescence quantum efficiency.

In the framework of this project, we have shown that it is possible to increase the writing resolution of multiphoton polymerization by employing Diffusion-Assisted DLW (DA-DLW), a scheme based on quencher diffusion, in a chemical equivalent of STED. This is based on the combination of a mobile quenching molecule with a slow laser scanning speed, allowing the diffusion of the quencher in the scanned area, the depletion of the generated radicals, and the regeneration of the consumed quencher. The material used as quencher is 2-(dimethylamino) ethyl methacrylate (DMAEMA), an organic monomer which is also part of the polymer structure. Due to its amine moieties, this is the same monomer we have employed in the past as a metal ligand, to enable the selective metallization of 3D photonic crystals.[4] Our approach was to fabricate 3D dielectric nanostructures containing the metal binding material DMAEMA, and subsequently selectively metallize them with silver using electroless plating (EP). EP is a fairly simple process that doesn't require any specialized equipment, and the metal deposition can be done without using any electrical potential. In general it is characterized by the selective reduction of metal ions at the surface of a catalytic substrate immersed into an aqueous solution of metal ions, with continued deposition on the substrate through the catalytic action of the deposit itself. Using DLW and selective EP, we successfully fabricated 3D metallic photonic crystals with bandgaps at optical wavelengths.
We have combined these two methodologies to fabricate 3D metallic and structures with complex geometries and sub-diffraction limit resolution. We fabricate woodpile and spiral photonic crystals and we show that they have well-defined diffraction patterns, indicating the quality of their fabrication and their internal periodicity. In addition, we have fabricated 3D structures decorated with gold nanoparticles. Such structures can be useful in applications such as biosensing.

Structure fabrication

Designs

In this project, we investigated four kinds of nanostructures.

a. Photonic crystals using the woodpile geometry. This consists of layers of one-dimensional rods with a stacking sequence that repeats itself every four layers. The distance between four adjacent layers is c and, within each layer, the axes of the rods are parallel to each other with a distance *d* between them. The adjacent layers are rotated by 90°. Between every other layer, the rods are shifted relative to each other

by *d/2*. For the case of $c/d = \sqrt{2}$, which was used in these experiments, the lattice can be derived from a face-centered-cubic (fcc) unit cell with a basis of two rods.

b. Silver-coated woodpile structures with a period of 600 nm. These type of structures were investigated theoretically and experimentally in reference [5], and they were found to have bandgaps at optical wavelengths.
c. Dielectric woodpile structures, also with period 600 nm, decorated with gold nanoparticles. These can be useful in applications such as biosensing, where thiol chemistry can be employed for biomolecule immobilization. [6]
d. Spiral photonic structures. These were modeled on the structures presented in Ref.7 by Ganzel and colleagues from KIT, Germany. In the KIT study, voids were fabricated into a positive photoresist using DLW, which were subsequently filled with gold using electroplating. Their structures were used as broadband polarizers. In our study, we have copied the spiral design and used a metal-binding negative photopolymer to re-create these spiral structures. As these spirals have high aspect ratio and it is difficult for them to remain free-standing during the sample development process, support structures were added to the design, as it will be shown in the results section.

Materials

The material used for the fabrication of the dielectric 3D structures is based on the organic-inorganic hybrid described earlier. [4] It has been produced by the addition of zirconium propoxide (ZPO, 70% in propanol) to methacryloxypropyl trimethoxysilane (MAPTMS). The monomer 2-(dimethylamino)ethyl methacrylate (DMAEMA) has been added as a quencher. MAPTMS, methacrylic acid (MAA) and DMAEMA were used as the organic photopolymerizable monomers, while ZPO and the alkoxysilane groups of MAPTMS served as the inorganic network forming moieties. Michler's ketone, 4,4-bis(diethylamino) benzophenone (BIS) was used as a photoinitiator.

For the fabrication of the metallic and gold-nanoparticle covered structures, he materials investigation, synthesis and metallization protocols employed have been described in detail previously in [4-5]. The silver-coated structures were fabricated using 30% DMAEMA [4], while the gold-nanoparticle covered ones 10% DMAEMA [8]. The gold nanoparticles were prepared following the metallization process described in [4], omitting the last plating step.

3D structure fabrication

The experimental setup employed for 3D structure fabrication has been described previously. A Ti:Sapphire femtosecond laser (Femtolasers Fusion, 800 nm, 75MHz, <20fs) was focused into the photopolymerisable composite using a high numerical aperture focusing microscope objective lens (100x, N.A. = 1.4, Zeiss, Plan Apochromat). Sample movement was achieved using piezoelectric and linear stages, for fine and step movement, respectively (Physik Instrumente). The whole DLW setup was computer-controlled using the 3DPoli software. The average power used for the fabrication of the high-resolution structures was 4.8 mW, measured before the objective, while the average transmission was 20%. The scanning speed was always set to 20μm/s.

Structural and optical characterization of the structures achieved

Angle Resolved Transmittance Measurements

Since the contrast in refractive index between the material and air is of the order of 0.5, the fabricated woodpile crystals do not possess a complete photonic bandgap. However, in certain directions a photonic stop-gap arises leading to a decrease in transmission. The transmission spectra of the woodpile structures stopgaps were measured using angle resolved transmittance microscopy. For this, a home-build setup was employed. Light from a Ti-Sapphire laser (800nm, 180fs, 1mJ/pulse, 1KHz repetition rate) was focused using an f = 3cm lens into a 3cm long cell filled with distilled water, in order to produce white light continuum, providing a useful broad spectral range of 450nm to 1000nm wavelength. The light was collimated and then focused on the sample. The sample was mounted to have accurate 3D and rotational control. Another lens coupled out the beam and, in combination with a lens, imaged the sample onto an intermediate image plane. This intermediate image plane was further imaged onto an IR/VIS fiber with a core diameter of 200 μm. The output of the fiber was connected to an optical spectrometer (Ocean Optics S2000), covering a spectral range from 300 nm to 1000 nm. The spectrum was recorded through a Labview-driven program. To ensure proper normalization, all the measured transmission spectra were normalized to the bare glass substrate for the same angle of incidence, requiring only a very small lateral movement of the sample. In order to align the sample appropriately on the optical axis, the intermediate image plane was imaged onto a CCD camera using a dichroic mirror. This also served to remove the 800nm pump laser beam of the continuum, thus avoiding saturation of the spectrum analyzer. The half-opening angle of the incident light was reduced to 5°, assured by iris diaphragms.

The diameter of the beam at the sample was 6 μm, while the measured nanostructure surface normal to the beam was typically 30 μm x 30μm. As the size of the sample's surface is comparable to the beam spot diameter, sample alignment is difficult and critical. To check the alignment, but also to check the quality of the sample, the diffraction pattern in the transmitted waves produced by the structure when illuminated by the white light beam were used. In general, diffraction patterns reveal structural characteristics, as well as, sample quality. Figure 2b shows a typical such diffraction pattern, generated by the woodpile structure of Figure 2a (Scanning Electron Microscopy (SEM) image, full structure and detail). To understand the diffraction pattern, one should note that the woodpile structure presents the (001) family of planes parallel to the crystal surface - the direction normal to these planes is referred as Γ*X*, which is the one studied. In these planes the structure presents a square symmetry, that is actually revealed by the square symmetry of the diffraction pattern observed.

Results

As already described by several groups, diffraction channels for normal incidence are open when the incident wave vector **k** is larger in magnitude than any of the 2D reciprocal lattice vectors, ***g***, of the planes parallel to the crystal surface. A diffraction cutoff is observed

whenever |**g**| = |**k**|. For a square lattice, writing **g** as a linear combination of a set of 2D primitive reciprocal lattice vectors ($\mathbf{b}_1$,$\mathbf{b}_2$), i.e. $\mathbf{g} = p\mathbf{b}_1 + q\mathbf{b}_2$, *p, q* integers, the cut-off condition is met for

$$\frac{d}{\lambda} = \frac{1}{n}\sqrt{p^2 + q^2}$$

where *n* is the refractive index of the diffraction medium, λ is the wavelength of the incident radiation and *d* is the periodicity in the planes perpendicular to the propagation direction. In air (*n* = 1) four diffraction channels open, corresponding to

$(p, q) = (1, 0)\ ,\ (0, 1)\ ,\ (-1, 0)\ ,\ (0,-1),$

when $\frac{d}{\lambda} \geq 1 \Rightarrow d \geq \lambda$.

In the same manner, a second set of diffraction spots appears for
$(p, q) = (1, 1)\ ,\ (1,-1)\ ,\ (-1, 1)\ ,\ (-1,-1)$
when $d > \sqrt{2}\lambda$.

As it can be seen in figure 2b, in the case of *d* = 1700*nm* the whole visible spectrum is diffracted as both conditions $d > \lambda$ *and* $d > \sqrt{2}\lambda$ hold, thus both sets of diffraction channels are observed. The first set of four diffraction spots form the characteristic cross round the forward transmitted beam, whereas the second set of diffraction spots appears along the diagonal directions. The diffraction cutoff starts to become more pronounced as one moves to unit cells close to the visible spectral range, such as for *d* = 600*nm* and *d* = 500*nm,* (Figure 3 and 4 respectively), where one can clearly observe the cut off for the "red part" of the visible. The same situation holds as one moves from *d* = 500*nm* to *d* = 400*nm* (Figure 5), where a cutoff exists for the "red" and the "green part" of the visible spectrum. As the second condition is not met for any visible wavelength for woodpiles with d > 600nm, no diagonal spots are observed in the diffraction patterns shown in figures 3c, 4c and 5c.
Furthermore, for the case of our woodpile structure with *d* = 400*nm*, the characteristic cross is not clearly seen. Instead of the four diffraction channels along two orthogonal directions, only two are observed along a single direction. However, the sharpness of the diffraction spots indicates the long-range order inherent to periodic photonic crystals due to their translational symmetry. This is in accordance to the SEM image taken, where structural deformation due to shrinkage is evident. This is further supported by the optical response measured (figure 5d). Theoretical calculations made using the MPB software package for rod width *w* = 0.176*c*, refractive index *n* = 1.52 and rod height *h* = 0.5*c* are shown schematically in figure 6e. The band-gap is located for a normalized frequency of c/λ~0.8, that is for a vacumn wavelength of ~ 710nm, which is about 100nm blue-shifted in relation to the transmittance dip measured experimentally (~820nm). In addition, the diffraction cutoff is

located at c/λ ~ 1.414 => d = 400nm, thus the other two set of spots may correspond to a higher order partial band-gap located at c/λ~0.966 and higher.

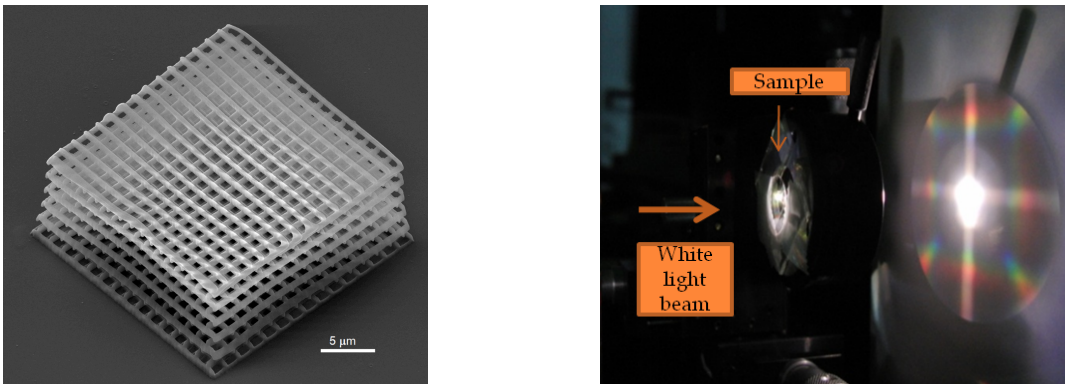

(a) (b)

Figure 2(a) A 3D woodpile structure with 1700 nm interlayer periodicity. (b) The diffraction pattern generated when a white-light beam goes through the woodpile structure

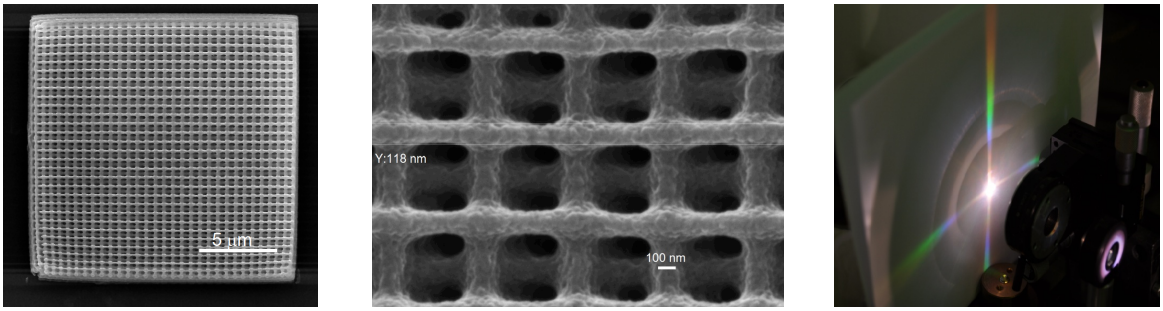

(a) (b) (c)

Figure 3 A 3D woodpile structure with 600 nm interlayer periodicity. (a) The whole structure, (b) structure detail, (c) the diffraction pattern generated when a white-light beam goes through the woodpile structure

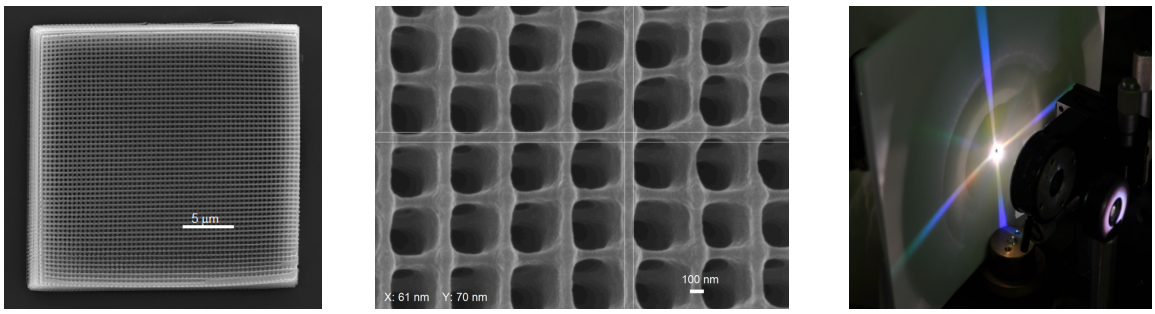

(a) (b) (c)

Figure 4 A 3D woodpile structure with 500 nm interlayer periodicity. (a) The whole structure, (b) structure detail, (c) the diffraction pattern generated when a white-light beam goes through the woodpile structure

It is worth noting in this case that the highest resolution achieved is of the order of 100 nm (Fig. 6b), lower than in the case of the 500 nm interlayer periodicity where the line width measured was approximately 70nm (Fig.5b). While the difference is small and not enough to draw any conclusions, this reduced resolution is possibly due to underexposed areas photopolymerizing due to radical diffusion.

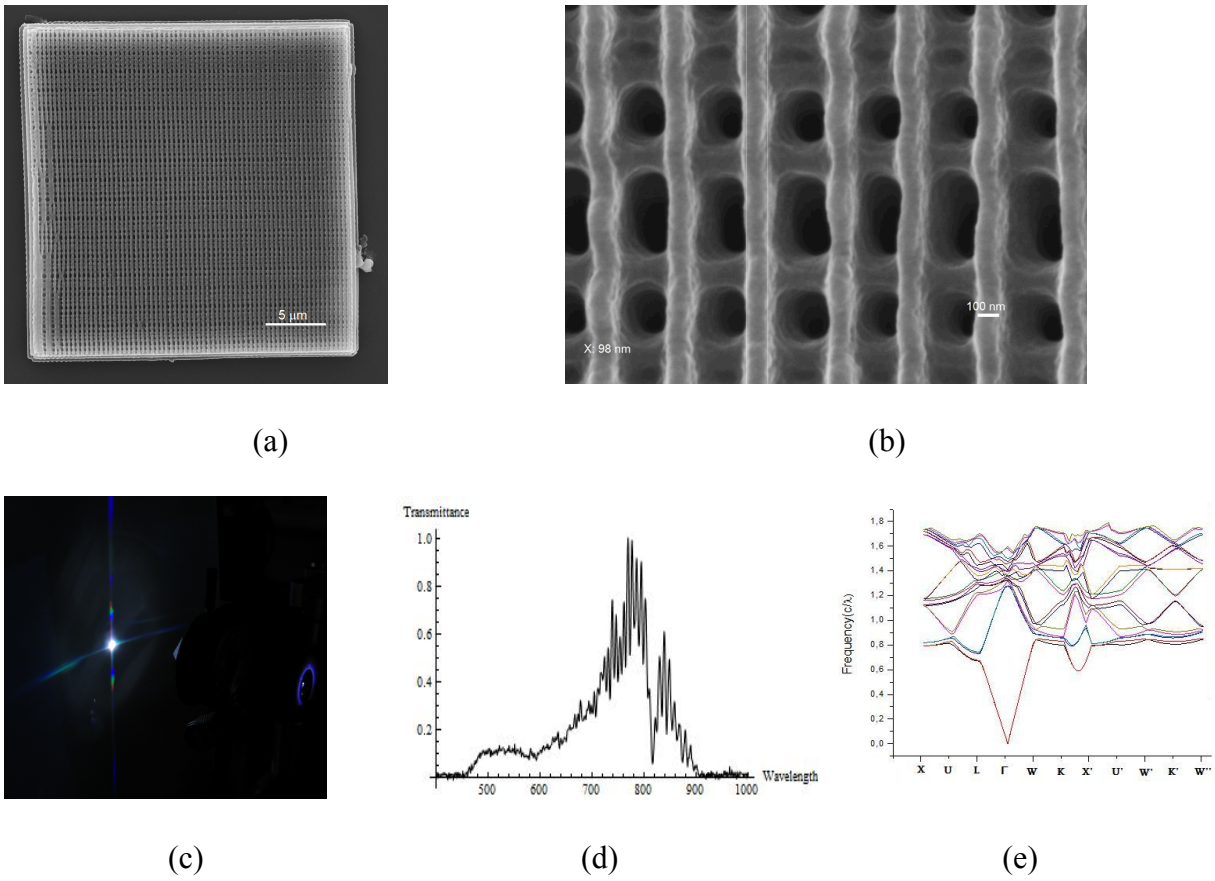

(a) (b)

(c) (d) (e)

Figure 5A 3D woodpile structure with 400 nminterlayer periodicity. (a) The whole structure, (b) structure detail, (c) the diffraction pattern generated when a white-light beam goes through the woodpile structure, (d) The measured bandgap and (e) the band calculations

Figure 6 shows a woodpile structure with 500nm interlayer periodicity, fabricated using the same material without the quencher. The fabrication conditions were kept the same as previously. In this case however, the intralayer gaps are fully polymerized, and the woodpile in fact is a solid polymer block, allowing us to conclude that the increased resolution is due to the quencher addition.

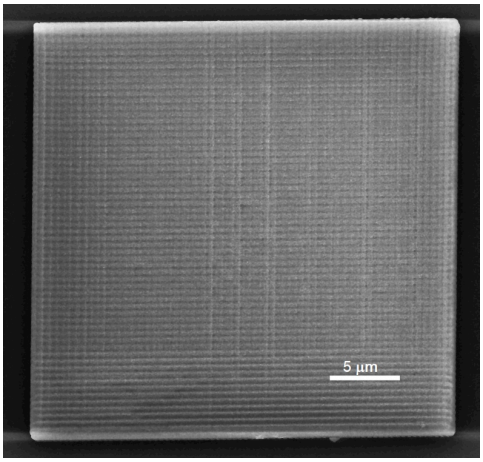

Figure 6 A 500 nm intralayer periodicity woodpile structure fabricated using the employed hybrid material without adding a quencher. In this case the interlayer gaps have fully polymerized, resulting in the structure being a solid block.

Figure 7a shows a Scanning Electron Microscopy (SEM) image of a woodpile structure with 600 nm period fabricated and metallized using the procedure described earlier. Figure 7b show a detail of such a structure. It can be seen that the resolution achieved is in the order of 100 nm.

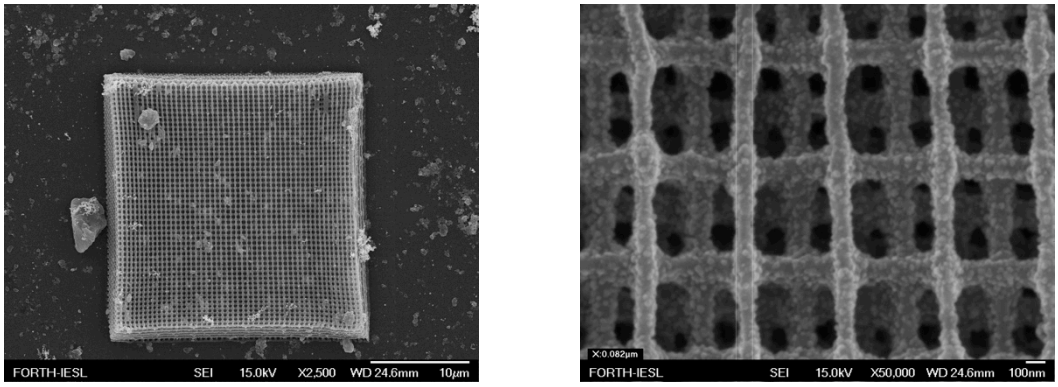

(a) (b)

Figure 7 Woodpile photonic crystals. (a) the whole structure (b) detail.

Figure 8 shows SEM images of woodpile structures decorated with gold nanoparticles. Figure 8a shows the whole structure, while Figure 8b shows a detail of such a structure, where the nanoparticles are clearly visible. The density of these nanoparticles can increase or decrease by increasing or decreasing the percentage of DMAEMA, respectively [4]. The size of the nanoparticles can be modified by altering the growing conditions. [4]

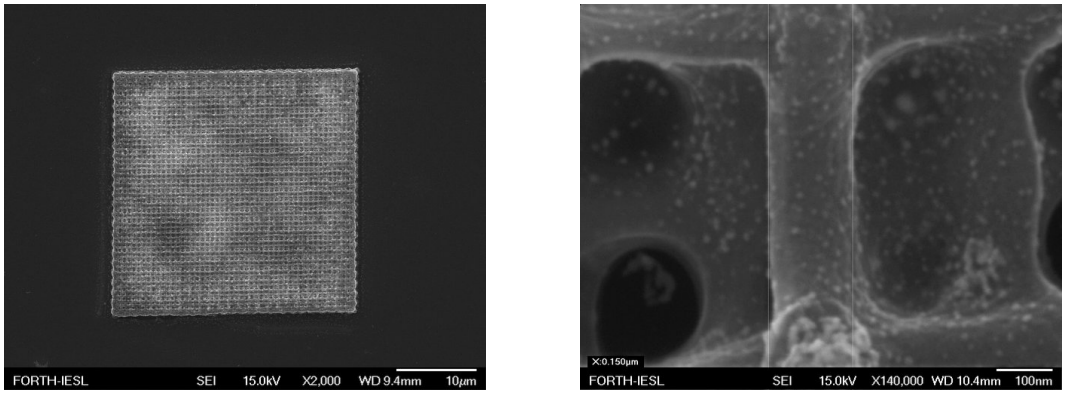

(a) **(b)**

Figure 8 Woodpiles decorated with gold nanoparticles (a) the whole structure (b) detail.

Figure 9 shows the Energy-dispersive X-ray (EDX) spectrogram of the woodpile structures, where the gold (Au) peaks are clearly visible.

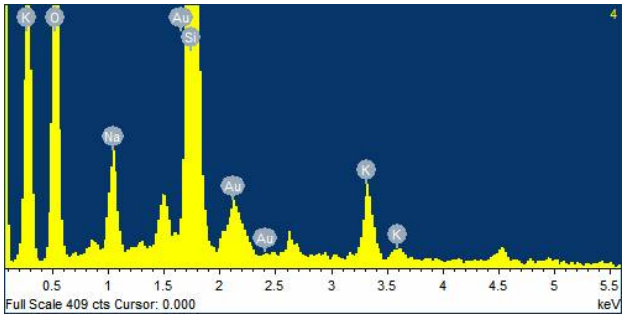

Figure 9 EDX spectrogram of the woodpile structures. The gold (Au) peaks are clearly visible

.

Figure 10 shows a series of dielectric and silver-coated spiral structures fabricated as described earlier. Figures 10(a) and 10(b) shows 14x14 arrays of spirals before silver coating, respectively. Support lines between the spirals are clearly visible. It is also clear that, even thought there is some debris on the glass substrate, the silver metallization is selective. Figure 10(c) shows a close SEM image of a spiral; the resolution achieved is in the order of 100 nm. In addition, the silver coating is fairly uniform, with no visible large silver grains. Figure 10(d) shows the diffraction pattern produced when the spirals were illuminated with white light. As it can be seen, the pattern is regular, symmetric, and has well-defined colours, indicating the periodicity of the structures. This periodicity is not disturbed by the support structures.

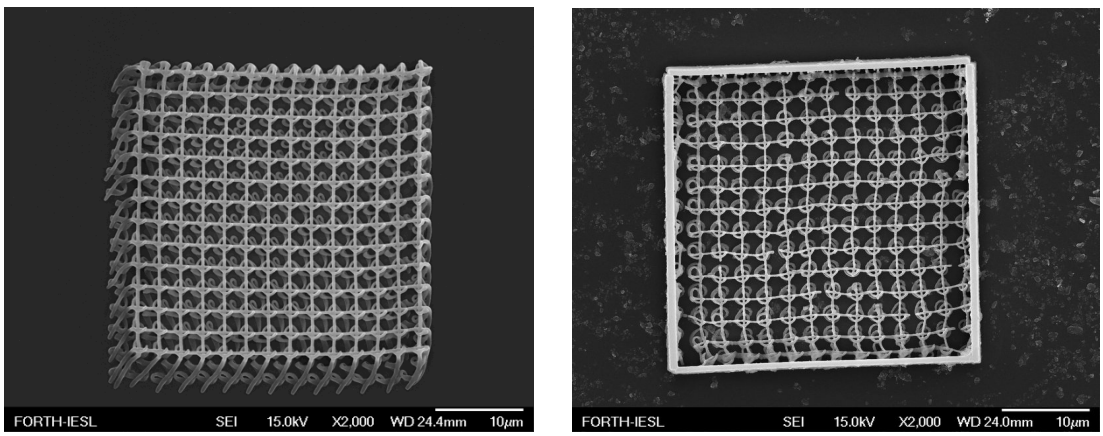

(a) (b)

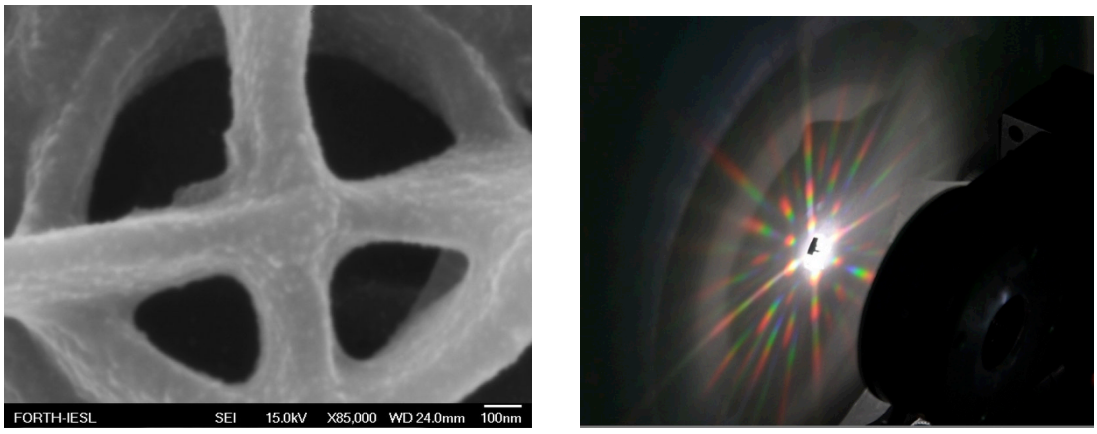

(c) (d)

Figure 10 Spiral photonic crystal structures. (a) An array of dielectric spirals (b) An array of metalized spirals (c) Detail of a spiral with lateral resolution is in the order of 100 nm. (d) The diffraction pattern generated when the structure is illuminated with white light.

Diffusion role in the DLW resolution

Diffusion is a non-local factor that, in application to DLW, can cause the energy of light absorbed in one domain of the medium to have a final effect in another domain. Hence, pronounced diffusion weakens the concept of a polymerization threshold, and thus diffusion can potentially help to overcome the limitation on making features at sub-diffraction distances. Whereas the diffusion of small radicals as well as macromolecules can be detrimental to spatial resolution, the diffusion of the quencher, which inhibits the polymerization, can have a positive effect.

One of the prominent positive effects of diffusion is the recovery of the initial quencher spatial concentration after irradiation. When writing two adjacent lines, the quencher in the interstice is consumed. When the lines are written at sub-diffraction distance to each other, the quencher in the interstice is totally consumed and the polymerization is started as though it was a single feature, as seen in Fig. 1b. However, when the quencher is recovered to its initial concentration before writing of the next neighbouring line such limitation of the spatial resolution is relaxed (Fig. 11).

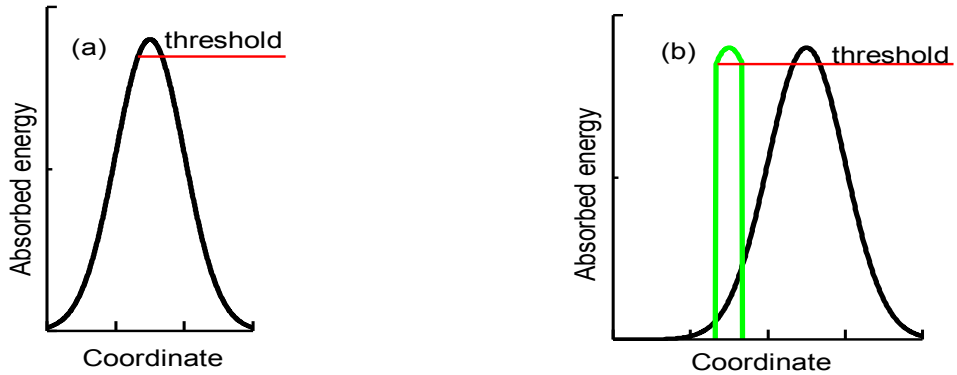

Figure 11 (a) Formation of a single feature. (b) Formation of the second feature at sub-diffraction distance from the first one assisted by quencher diffusion. The energy absorbed during the first scan causes both the consumption of the quencher and formation of the polymer feature. Since the quencher is diffusion-regenerated between scans, the only effect of the irradiation that remains is the formation of the polymer feature (green line). This allows creation of the second feature at the sub-diffraction distance.

In our experiments, the addition of a quencher causes major improvement in the spatial resolution of written lattices. This means that the quencher not only changes the level of the polymerization threshold, but it affects also the polymerization non-locally due to diffusion. The quencher used, DMAEMA, is not attached to the inorganic network, so, it can diffuse. The time needed to write a single line of length $l_{line} = 30\mu m$ within the photonic crystal with scanning velocity $v = 20\mu m/s$ is $t_{line} = 1.5s$. As the diffusion coefficient of DMAEMA is $D_Q=10^{-5}$-10^{-8}cm^2/s, the estimated time of diffusion of it at the distance of $d_{period} = 400nm$ between the lines becomes $t_{diff\,1} = d_{period}^2 / D_Q = 1.6 \cdot 10^{-4} \div 1.6 \cdot 10^{-1}\ s = 10^{-1} s$. That is, $t_{diff\,1} << t_{line}$, and therefore the quencher initial concentration recovers between line scans.

With N.A.=1.4 and λ=800nm the beam radius is r_{beam}≈180 nm. Therefore, the irradiation time of a particular point is $t_{\mathrm{irr}} = 2r_{\mathrm{beam}}/v = 8 \cdot 10^{-2}$ s. The estimated time of diffusion of DMAEMA through the irradiated domain is $t_{diff\,2} = r_{beam}^2 / D_Q = 3.2 \cdot 10^{-5} \div 3.2 \cdot 10^{-2}\ s = 10^{-1} s$. That is, $t_{diff\,2} < t_{irr}$, and thus diffusion is important during single line scans as well.

To understand the effect of the quencher diffusion during the line scans, let us now consider a basic photopolymerization model. The evolution of the spatial distributions of the number densities of the quencher molecules (Q), free radicals (R) and free monomer molecules (M) can be modeled by the following equation set:

$$\frac{\partial R}{\partial t} = S(\vec{r},t) - k_{tQ} Q R, \qquad (1)$$

$$\frac{\partial Q}{\partial t} = D_Q \Delta Q - k_{tQ} Q R, \qquad (2)$$

$$-\frac{\partial M}{\partial t} = k_p R M, \qquad (3)$$

Free radicals are generated as a result of the absorption of laser light by the photoinitiator. For two-photon absorption, the source term is proportional to the square of the local field intensity, I, pulse duration t_{p} and pulse repetition rate R_{p}: $S \propto I^2(\vec{r},t)\, t_p R_p$. As a result of the quenching reaction, both the quencher and the radical are consumed with the

reaction rate k_{tQ}. The diffusion coefficient of the quencher is D_Q , Δ is the Laplacian. The polymerization rate is given by Eq. (3) being proportional to the monomer number density, M , the radical number density and the propagation constant k_p. The conversion

$$p = \frac{M_0 - M}{M_0},$$

indicates the degree of polymerization (here, M_0 is the starting number density of the monomer).

Since the line scan is much slower than the diffusion of the quencher, i.e. $t_{diff\,2} << t_{irr}$, one can consider long-lasting irradiation with constant in time point-like source. For simplicity, we take the spherically symmetric Gaussian source:

$$S = S_0 \exp\left(-r^2/2L^2\right) \qquad (4)$$

Due to diffusion, the consumption of the quencher in the irradiated volume can be compensated by its transfer from non-irradiated domains. In such a balanced state the quencher number density distribution is maintained constant in time: $\partial Q/\partial t \equiv 0$. Examples of such calculated distributions are shown in Fig. 12.

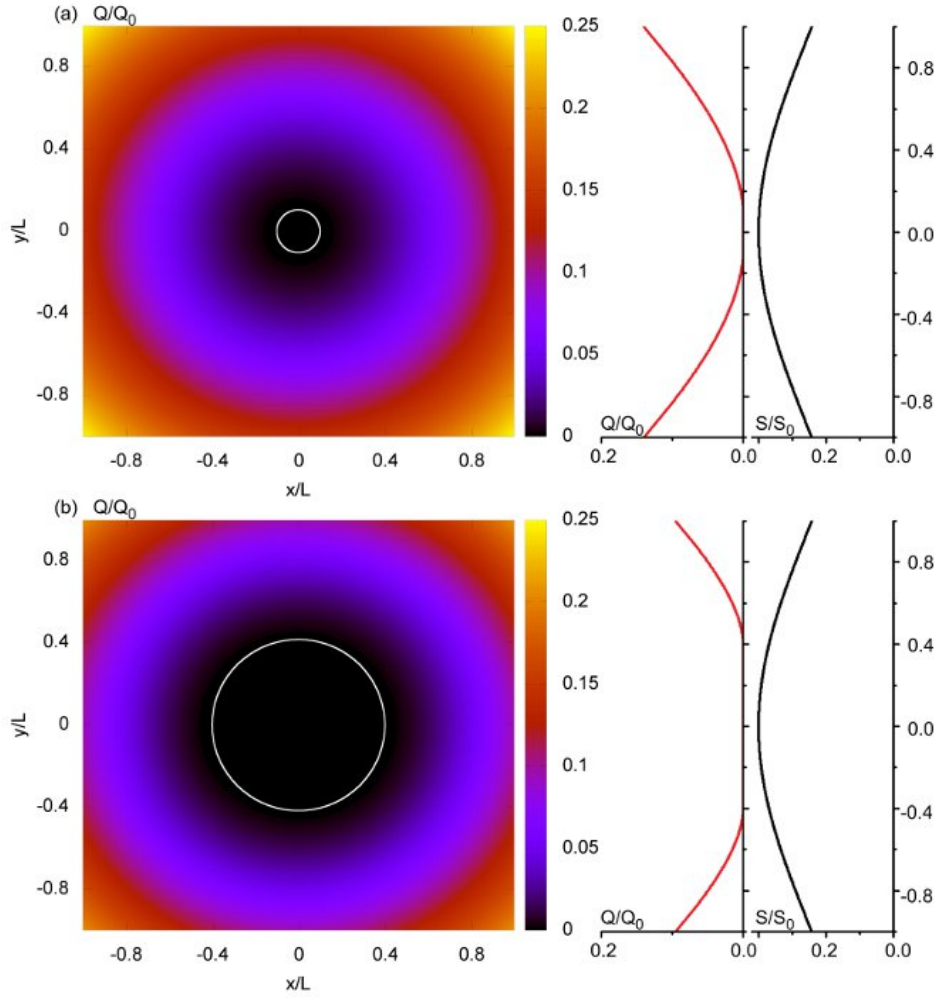

Figure 12Calculated distributions of the quencher number density Q with respect to the initial quencher number density Q_0 (color maps and red line graphs). L is the width of the Gaussian radical source. Radii of the quencher-free domains (indicated with white circles) are $0.1 \cdot L$ (a) and $0.4 \cdot L$ (b). Ratio of the magnitudes of the laser beam intensity between cases (b) and (a) is $I_b / I_a \approx 1.038$. The distributions of the source of the radicals are plotted with black lines.

It can be seen that there is no quencher in the central domain of the irradiated volume. The polymerization is inhibited only in the region that surrounds this domain. This effect is similar to the one reached in STED-DLW, however, in our case, one does not need any depletion beam.

By solving Eqs. (1-2) for the case of Gaussian radical source (4) one can analytically obtain the radius of the quencher-free domain:

$$r_1 = L\sqrt{2\ln\left(\frac{S_0 L^2}{Q_0 D_Q}\right)}, \qquad (5)$$

where Q_0 is initial quencher number density. It can be seen that the radius can be made arbitrarily small by tuning the laser beam intensity, since the radical source magnitude is $S \propto I^2(\vec{r},t)\, t_p R_p$. The irradiation time, conversely, does not affect the size of the quencher-free domain. An increase in the irradiation time (or a decrease in the scan speed) only causes the increase in the polymerization degree (conversion) within the quencher-free domain. Contrary, in the threshold model (without quencher diffusion), the maximal polymerization degree of a nanofeature can be increased by applying higher irradiation dose either by increasing beam intensity or irradiation time (Fig.13). However, the higher dose inevitably results in increase of the size of the polymer feature. By employing the diffusion of the quencher, on can handle both the size and the maximal conversion of the polymer feature separately. Formation of sharp spatial distributions of the conversion is important for achieving high spatial resolution, high mechanical stability and stability against fluctuations.[36]

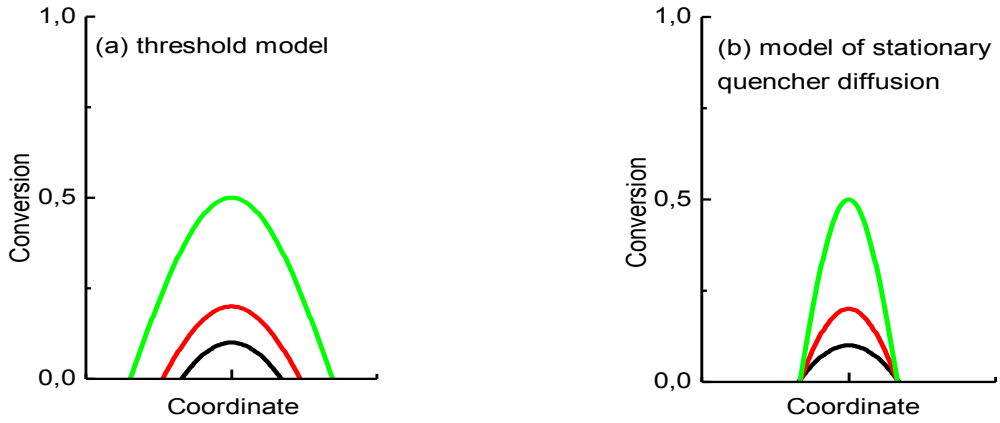

Figure 13(a) Schematic representation of conversion profiles in threshold polymerization regime for different irradiation dozes. (b) Schematic representation of conversion profiles in model of stationary quencher diffusion for different irradiation times and fixed irradiation intensity.

The model presented above has not taken into account the temperature and gel viscosity, parameters that would increase and decrease the diffusivity of the quencher, respectively. In addition, the size of the quencher is a major factor; a smaller quencher would diffuse faster. A more detailed modeling of polymerization with diffusing quencher is planned for a future publication.

This new method based on quencher diffusion does not possess the stringent material requirements of STED-DLW, it does, however impose certain limitations. The most important one is writing speed, as it is required that the laser scanning speed allows enough time for the quencher to diffuse. This could become an issue in the fabrication of larger structures if liquid photopolymers are used, due to thermal drift or other destabilizing factors.

Fortunately, most hybrid materials, like the one used here, have gel form and thermal drift or displacement is not a problem.

Summary/Conclusions

We have presented our research into improving the resolution of three dimensional structures by using a combination of a quenching monomer with slow laser scanning speed. We have fabricated woodpile structures with interlayer period 400 nm, comparable to what has been achieved by DLW-STED, considered today as 'state-of-the-art'. In addition, we have proposed a mechanism for this improved resolution. We have characterized the woodpile structures using angled-resolved transmission microscopy and we have shown that they exhibit long range periodicity and near-infrared stopgaps. The materials we use are readily available. While the method we propose does not allow the voxel shape control that DLW-STED does, we believe it offers an attractive alternative to high resolution 3D photopolymer structuring.

References

1. Farsari, M.; Vamvakaki, M.; Chichkov, B. N., Multiphoton Polymerization of Hybrid Materials. *J.Opt.* **2010,** *12*, 124001.
2. Fischer, J.; Wegener, M., Three-Dimensional Direct Laser Writing Inspired by Stimulated-Emission-Depletion Microscopy. *Opt. Mater. Express* **2011,** *1*, 614-624.
3. Hell, S. W.; Wichmann, J., Breaking the Diffraction Resolution Limit by Stimulated Emission: Stimulated-Emission-Depletion Fluorescence Microscopy. *Opt. Lett.* **1994,** *19*, 780-782.
4. Terzaki, K.; Vasilantonakis, N.; Gaidukeviciute, A.; Reinhardt, C.; Fotakis, C.; Vamvakaki, M.; Farsari, M., 3D Conducting Nanostructures Fabricated Using Direct Laser Writing. *Opt. Mater. Expr.* **2011,** *1*, 586-597
5. Vasilantonakis, N.; Terzaki, K.; Sakellari, I.; Purlys, V.; Gray, D.; Soukoulis, C. M.; Vamvakaki, M.; Kafesaki, M.; Farsari, M., Three-Dimensional Metallic Photonic Crystals with Optical Bandgaps. *Adv. Mater.* **2012,** *24*, 1101-1105.
6. Kabashin, A. V.; Evans, P.; Pastkovsky, S.; Hendren, W.; Wurtz, G. A.; Atkinson, R.; Pollard, R.; Podolskiy, V. A.; Zayats, A. V., Plasmonic nanorod metamaterials for biosensing. *Nat.Mater.* **2009,** *8* (11), 867-871.
7. Gansel, J. K.; Thiel, M.; Rill, M. S.; Decker, M.; Bade, K.; Saile, V.; von Freymann, G.; Linden, S.; Wegener, M., Gold Helix Photonic Metamaterial as Broadband Circular Polarizer. *Science* **2009,** *325* (5947), 1513-1515.
8. Sakellari, I.; Kabouraki, E.; Gray, D.; Purlys, V.; Fotakis, C.; Pikulin, A.; Bityurin, N.; Vamvakaki, M.; Farsari, M., Diffusion-Assisted High Resolution Direct Femtosecond Laser Writing. *ACS Nano* **2012,** *6* (3), 2302-2311.